Remeshed Smoothed Particle Hydrodynamics Simulation of the Mechanical Behavior of Human Organs

Simone E. Hieber, Jens H. Walther and Petros Koumoutsakos*

Institute of Computational Science

ETH, Zürich, Switzerland

*corresponding author, complete address:

Institute of Computational Science

Hirschengraben 84

ETH Zentrum

8092 Zurich, Switzerland

Tel no. +41 1 632 5258

Fax no. +41 1 632 1703

Email: petros@inf.ethz.ch

In computer aided surgery the accurate simulation of the mechanical behavior of human organs is essential for the development of surgical simulators. In this paper we introduce particle based simulations of two different human organ materials modeled as a linear viscoelastic solids. The constitutive equations for the material behavior are discretized using a particle approach based on the Smoothed Particle Hydrodynamics (SPH) method while the body surface is tracked using level sets. A key aspect of this approach is its flexibility which allows the simulation of complex time varying topologies with large deformations. The accuracy of the original formulation is significantly enhanced by using a particle reinitialization technique resulting in remeshed Smoothed Particle Hydrodynamics (rSPH). The mechanical parameters of the systems used in the simulations are derived from experimental measurements on human cadaver organs. We compare the mechanical behavior of liver- and kidney-like materials based on the dynamic simulations of a tensile test case. Moreover, we present a particle based reconstruction of the liver topology and its strain distribution under a small local load.

---

1. Introduction

The modeling and simulation of human organs such as soft biological tissue is important for a variety of medical applications including surgical planning, training and assistance through a surgery simulator based on virtual reality concepts [18]. The modeling and the simulation of soft biological tissue traditionally involve formulations using mass-spring models [19], or finite-element methods [5]. Mass-spring systems have been popular due to their easy implementation and low computational cost for real-time applications. However, the relationship between the true material properties of the organs and the structure of the mass-spring network and its parameters is a subject of extensive experimentation.

Finite Element Methods (FEM) are commonly used for simulations of deformable bodies in continuum mechanics. Due to their computational cost ordinary finite elements methods are not used often for real-time application. However, when the tissue is restricted to be a linear elastic material, it is possible to achieve real-time performance using only a limited number of nodes [5]. When considering nonlinear elasticity the finite element method leads, in general, to an implicit equation that needs to be solved iteratively, thus hindering real-time implementations. In addition when considering virtual surgery simulations involving cut surfaces and fluid-structure interactions the use of adaptive finite element methods requires a significant computational cost to resolve changes in the geometry and material properties.

Particle based methods such as vortex methods [4] and Smoothed Particle Hydrodynamics (SPH) [7, 13, 14] aim to bridge the gap between the efficient but low order mass-spring models with the high accuracy, but computationally expensive finite-element methods. Vortex and SPH methods approximate the governing partial differential using particles as computational elements. The material field quantities are represented by a linear superposition of the material quantities carried by the particles and weighted by a smooth interpolation kernel. The method is inherently adaptive as particle attributes (strength, locations) evolve according to their material time derivatives. However, the deformations associated with standard particle methods often lead to large inaccuracies of the quantities that are been simulated. In order to circumvent this problem remeshing of particle methods using moment conserving schemes was introduced in [11]. The moment conserving remeshing schemes developed in [10] have been then applied in the

context of SPH resulting in the method of Remeshed SPH (rSPH) [1]. rSPH involves a simple reinitialization technique of the particle locations (remeshing) whose strengths are adjusted so as to conserve moments of the resolved field quantities. Some advantages of our implementation include the possibility of a unified approach for treating fluids and solids and the flexible handling of complex topologies because no explicit connectivity information of the computational elements needs to be provided [8].

The present paper describes the fundamental numerical formulation by considering the rSPH solution of dynamic solid mechanics problems. We present results from one-dimensional solid-structure interactions and from deformation simulations of liver- and kidney-like materials based on a linear viscoelastic solid model for small deformations. In our simulations the Young's modulus is chosen according to experimental results [15], where aspiration experiments on human cadaver livers and kidneys, were used to derive the relaxation modulus.

2. Governing equations and SPH formulation

2.1. Mathematical model of the soft biological tissue

The mechanical behavior of soft biological tissue is modeled as a linear viscoelastic material for small strains. The governing equations are based on the conservation laws of continuum mechanics for mass and momentum

$$\frac{D\rho}{Dt} = -\rho \nabla \cdot \underline{v} \ , \tag{1}$$

$$\rho \frac{D\underline{v}}{Dt} = \nabla \cdot \underline{\underline{\sigma}} + \underline{f}_{ext} \, , \tag{2}$$

where ρ is the density, $\underline{v}$ the velocity field, $\underline{\underline{\sigma}}$ the Cauchy stress tensor, $\underline{f}_{ext}$ external body force, and $\frac{D}{Dt}$ denotes the material derivative

.

$$\frac{D}{Dt} = \frac{\partial}{\partial t} + \underline{v} \cdot \nabla, \tag{3}$$

$$\frac{d\underline{x}}{dt} = \underline{v}, \tag{4}$$

where $\underline{x}$ denotes the location of the material elements. The stress tensor depends on the constitutive model of the considered material. Here, we approximate the biological material as a linear viscoelastic solid. The solid model is based on Hooke's law [2] extended by Kelvin-Voigt damping model [9]. Thus, the components s_{ij} of the stress tensor $\underline{\underline{s}}$ depend linearly on the components e_{ij} of the Cauchy Green strain tensor $\underline{\underline{e}}$,

$$s_{ij} = 2m(e_{ij} + Te^{\cdot}_{ij}) + l d_{ij}(e_{kk} + T\dot{e}_{kk}). \tag{5}$$

The indices i, j, k =1, 2, 3 follow the Einstein's summation convention and d_{ij} is the Kronecker symbol. The time constant T is the relaxation time, and the Lamé constants μ, ? are defined by

$$\begin{aligned} m &= \frac{E}{2(1+u)}, \\ l &= \frac{uE}{(1-2u)(1+u)}, \end{aligned} \tag{6}$$

where *E* represents the Young's modulus and ? the Poisson's ratio. For small deformations the strain tensor $\underline{\underline{e}}$ evolves according to the deformation rate

$$\frac{D\underline{\underline{e}}}{Dt} = \tfrac{1}{2}(\nabla\underline{v} + (\nabla\underline{v})^T). \tag{7}$$

The boundary of an elastic material can be fixed or moved with a prescribed velocity. Alternatively, it can be stress-free or exposed to a mechanical load.

2.2. Smoothed Particle Hydrodynamics (SPH)

In Smoothed Particle Hydrodynamics the elastic material is discretized onto particle carrying information about their position, velocity, mass, density, strain and stress. The particles move according to their velocity $\underline{v}$ and their position $\underline{x}$ changes as governed by Eq. (4).

In the SPH approximation any field quantity A is interpolated at a position r by a weighed sum of contributions from all particles:

$$A(r) = \sum_b A_b \, V_b \, W(r - r_b, h), \tag{8}$$

where the summation extends over all particles, A_b denotes the function value at the location of the b-th particle, and V_b the volume of the b-th particle. The smoothing kernel W(r, h) is a mollifying approximation of the Dirac-function, i.e.

$$d(x) = \lim_{h \to 0} W(x, h), \tag{9}$$

where h is the smoothing length. In the present implementation, a quartic spline kernel is used constructed by B-splines having continuous first, second and third derivatives [1]. The smoothing length h is set to be $1.25\Delta x$, where Δx is the initial particle spacing. The derivative of any interpolated function A can be derived by differentiation of Equation (8) applying the derivative to the smoothing kernel W(x, h). For a conservative formulation a symmetric form is used when computing spatial derivatives, thus let $\left\langle \frac{\partial A}{\partial x_i} \right\rangle_a$ denote the particle approximation of the first derivative of the a-th particle located at r_a [14], then

$$\left\langle \frac{\partial A}{\partial x_i} \right\rangle_a = \sum_b V_b \left(A_b - A_a \right) \cdot \frac{\partial}{\partial x_i} W \left(r_a - r_b, h \right). \tag{10}$$

By applying Equation (10) to the conservation equations (1) and (2) we obtain

$$\left\langle \frac{Dr}{Dt} \right\rangle_a = -r_a \sum_b V_b \left(\underline{v}_b - \underline{v}_a \right) \cdot \nabla_a W \left(\underline{x}_a - \underline{x}_b, h \right), \tag{11}$$

$$\left\langle r \frac{D\underline{v}}{Dt} \right\rangle_a = \sum_b V_b \left(\underline{\underline{s}}_b - \underline{\underline{s}}_a \right) \cdot \nabla_a W \left(\underline{x}_a - \underline{x}_b, h \right). \tag{12}$$

The strain evolution equation (7) becomes

$$\left\langle \frac{D\underline{\underline{e}}}{Dt} \right\rangle_a = \frac{1}{2} \left[\sum_b V_b \left(\underline{v}_b - \underline{v}_a \right) \cdot \nabla_a W \left(\underline{x}_a - \underline{x}_b, h \right) + \left[\sum_b V_b \left(\underline{v}_b - \underline{v}_a \right) \cdot \nabla_a W \left(\underline{x}_a - \underline{x}_b, h \right) \right]^T \right]. \tag{13}$$

2.3. Stress-free boundary condition

The stress-free boundary condition implies that the surface traction $\underline{t}$ is equal to zero:

$$\underline{t} = \underline{\underline{s}}_s \underline{n}_s = \underline{0}, \tag{14}$$

where $\underline{\underline{s}}_s$ is the stress tensor on the surface and $\underline{n}_s$ the surface normal. Previous implementations of the stress-free boundary condition in two dimensions involved the manipulation of the stress tensor rotated into local coordinate system oriented according to the surface normal [16, 17]. In three dimensions the

determination of the local coordinate system and the forward and backward rotations are computationally expensive operations. We avoid these operations by using a penalty force. We evaluate the surface traction $\underline{t}_p$ on the boundary particles as the product of the particle stress tensor $\underline{\underline{s}}_p$ and its surface normal (cf. Eq. (14)) . According to this surface traction we apply a body force (cf. Eq. (2)) to the boundary particle to cancel the surface traction.

The surface normal $\underline{n}_s$ is determined by a hybrid particle level-set method. In the hybrid particle level-set method the particles carry the distance F to the material surface and the unit surface normal $\underline{n}_s$ on the particle is approximated by

$$\underline{n}_p = \frac{\langle \nabla \Phi \rangle_p}{\left| \langle \nabla \Phi \rangle_p \right|}. \tag{15}$$

During the simulation the distance field F moves with the particles and gets distorted. Due to the small deformations of the material, however, it is not necessary to re-initalize the distance field F .

3. Remeshing

To secure the convergence of the method the particle map must be regular [4]. This is achieved by a reinitialization scheme (remeshing) in which the conserved quantities are redistributed onto a new set of particles with the spacing Δx . The quantities are interpolated by the smooth interpolation kernel M'4 of 3rd order:

$$M'4(r,\Delta x) = \begin{cases} 1 - \dfrac{5s^2}{2} + \dfrac{3s^3}{2} & 0 \le s < 1, \qquad s = \dfrac{|r|}{\Delta x} \\ \dfrac{(1-s)(2-s)}{2} & 1 \le s < 2, \\ 0 & s \ge 2. \end{cases} \tag{16}$$

$$Q_{new}\left(\underline{x}_{new}\right)=\sum_{b} Q_b \; M'4\left(x_{new}-x_b,\Delta x\right)M'4\left(y_{new}-y_b,\Delta x\right)M'4\left(z_{new}-z_b,\Delta x\right) \tag{17}$$

The interpolated quantity Q must be a conserved extensive property of the particle. In this study the particle quantities of the linear viscoelastic solid are mass, momentum and the product of strain components and volume. The quantities of the new particles are interpolated in three dimensions by using a tensorial product of the remeshing kernel M'4.

Fig. 1, Fig. 2 and Fig. 3 demonstrate the effect of remeshing particles in a simple deformation test case [6]. A sphere of radius 0.15 placed within a unit computational domain at (0.35, 0.35, 0.35) is driven by a three dimensional velocity field

$$v(x,y,z)=\begin{pmatrix} 2\sin^2(p\,x)\,\sin(2p\,y)\,\sin(2p\,z) \\ -\sin(2p\,x)\,\sin^2(p\,y)\,\sin(2p\,z) \\ -\sin(2p\,x)\,\sin(2p\,y)\,\sin^2(p\,z) \end{pmatrix} \tag{18}$$

From the initial set of 40x40x40 particles uniformly distributed in a unit domain, particles outside the sphere are rejected before the convection, which results in a set of about 900 particles. Fig. 1 and Fig. 2 show the particle solution without and with remeshing, at T=0.0, 0.4 and 0.6. In the final frames at T=0.8 (Fig. 3) the deformation has teared the object apart whereas the remeshed object still shows a non-ruptured surface.

4. Fluid-structure interactions

Often, organs interact with fluids, such as blood in a vessel or air in the lungs. Therefore we also consider fluid-structure interactions for biological systems. Here we start with a one dimensional test case where a linear elastic solid interacts with a viscous fluid. The fluid is described through the Burger's equation and

the solid by a one-dimensional wave equation. We solve a unified formulation of this system [8] as recently proposed by Cottet [3] . Thus, the fluid velocity u(x,t) and the solid displacement d(?,t) is governed by

$$\frac{\partial u}{\partial t}+u\frac{\partial u}{\partial x}=-\frac{1}{2}c^F u\frac{\partial u}{\partial x}+\left(c^F+\frac{\partial x}{\partial x}c^S\right)\frac{\partial}{\partial x}\left(u\frac{\partial u}{\partial x}c^F+m\frac{\partial d}{\partial x}c^S\right) \tag{19}$$

where c^F and c^S are characteristic functions defining the fluid and solid domain, respectively. The Eulerian coordinate x and the Lagrangian coordinate ? are related through $x(x,t)=x+d(x,t)$.

We set solid elasticity coefficient μ=1 and the solid elasticity coefficient ?=0.001. Initially the fluid is located in the interval [-0.5,0] and the solid in [0,0.5]. The initial conditions are

$$\begin{aligned} d(x,0)&=0,\\ u(x,0)&=-0.1(\cos(2p\,x)+1). \end{aligned} \tag{20}$$

The imposed boundary conditions require the materials to be at rest at the outer limits of the computational domain and are expressed by

$$\begin{aligned} u(-0.5,t)&=0,\\ d(0.5,t)&=\frac{\partial d(0.5,t)}{\partial t}=0. \end{aligned} \tag{21}$$

In our test case the map of the solid particles remains uniform and the reinitialization scheme is only applied to the fluid particles conserving the particle momentum. To approximate the particle derivatives at the interface we use one-sided differentiation. Fig. 4 shows the velocity profiles of a rSPH and an ALE solution using 100 computational elements. The results show that the particle method is more robust that the ALE method with the ALE method overshooting in fluid regions with high velocity gradients. When compared to a high resolution particle simulation with 400 particles, the rSPH method is more accurate

than the ALE solution with L^2-errors of 0.04 and 0.14, respectively. The extension of this approach to higher dimensions is presently under consideration.

5. Results

5.1. Determination of material parameters

The Young's modulus needed to determine the Lamé constants in Equation (7) is obtained from experimental results [15]. Based on the aspiration experiments on human cadaver livers and kidneys, the relaxation modulus E(t) was determined. As an approximation we chose the Young's modulus, E as the limit of the relaxation modulus when time goes to infinity to ensure the same stationary solution. The values of the Young's moduli we used are 0.1MPa for the liver and 0.01MPa for the kidney. Due to the high water content of the organs the density can be approximated by the density of water (1000 kg/m^3) in all cases. The relaxation times (T) is chosen large enough to prevent oscillations (here $T_{Liver} = 0.2$, $T_{Kidney} = 0.2$). A Poisson's ratio of 0.3 is used.

5.2. Simulation of human organs

Tensile test cases were conducted on an initially undeformed unit cube of elastic material. All physical quantities are normalized by their characteristic values (density r_0 =1000kg/m^3, length x_0 =1m, time T_0 =1s). A cubic domain discretized with 343 particles is fixed on the bottom, and a normalized load of 1 is applied to the top. The simulations where performed on an AMD Athlon 1.5 GHz PC with 1024 MB RAM. For the time integration, we use a fourth order Runge-Kutta scheme with a normalized timestep of 0.001 for the liver and 0.0001 for the kidney material. The computations run at a rate of 25 timesteps per second. Fig. 5 shows the resulting time history of the extension of the liver and kidney material computed as the displacement of the top particles divided by the original length of the cube. At the beginning of the simulation the acceleration of the top is very high due to lack of internal forces. The motion of the particles creates strain resulting in a stress distribution which acts against the load. The displacement is approaching

a stationary level where load and surface traction balances each other. The viscosity of the material dissipates kinetic energy and prevents the solid from oscillating. Since the liver is much stiffer than the kidney the displacement of the liver cube is much smaller than the one of the kidney cube under the same load.

Fig. 6 shows the 3D surface reconstruction of a virtual liver discretized by 144 particles. The liver topology shown in Fig. 6 was originally described as a triangular mesh segmented from images data of the Visible Human Project ®. The internal liver structure is very complex, containing a huge network of functional cell groups (muralia) riddled with blood vessels. Therefore, the entire liver structure is not resolvable with today's simulation techniques and as a first approximation, we consider the liver as a isotropic elastic material. The interior of the liver was sampled into a uniformly distributed set of particles carrying the same mass and density. The visualization of the liver surface is performed by rendering an isosurface of the zero level set triangulated by the marching cube algorithm [12]. Although only a small number of particles is used and some anatomical details are lost the topology of the liver is well recognizable. A very small load (270 Pa) was applied to the upper-right part of the liver body by smearing out a local load pushing the surface to the bottom of the liver body. The load caused the very small deformations that are not noticeable when comparing the topology. Fig. 7 shows the resulting normal strain distribution on the liver surface in grayscale at an early transient state.

6. Conclusions

We presented rSPH to simulate solid-fluid interactions as they occur in biological systems. We report preliminary results in implementing particle based simulations in the context of rSPH in order to compare the mechanical behavior of human liver- and kidney-like materials under the same mechanical constrains. A particle-level set reconstruction of a liver topology is presented based on a low resolution particle discretization. A simulation of the mechanical behavior of the liver was performed by applying a small load to the surface.

Current research is directed in analysing the convergence, the stability and robustness of the simulations along with large scale simulations and a validation from experimental results. Beyond the realm of linear elasticity we will be employing rSPH to handle large scale organ deformations.

7. Acknowledgements

The authors wish to acknowledge several helpful discussions with Dr. A. Chaniotis, ETH Zurich, Switzerland. We gratefully acknowledge the support from the National Center of Competence in Research CO-ME, Switzerland. We wish to thank the Computer Vision Laboratory, ETH Zurich, for providing the liver topology.

8. References

[1] A. K. Chaniotis, D. Poulikakos, and P. Koumoutsakos, Remeshed Smoothed Particle Hydrodynamics for the Simulation of Viscous and Heat Conducting Flows, Journal of Computational Physics, 182 (2002), pp. 67-90.

[2] T. J. Chung, Applied Continuum Mechanics, Cambridge University Press, 1996.

[3] G. H. Cottet, A particle model for fluid-structure interaction, C.R. Acad. Sci. Paris, Ser. I (2002), pp. 833-838.

[4] G. H. Cottet and P. Koumoutsakos, Vortex Methods: Theory and Practice, Cambridge University Press, 2000.

[5] G. Debunne, M. Desbrun, M.-P. Cani, and A. Barr, Dynamic Real-Time Deformations using Space & Timing Adaptive Sampling, Conference proceedings, SIGGRAPH 2001, Los Angeles, 2001.

[6] D. Enright, R. Fedkiw, J. Ferziger, and I. Mitchell, A hybrid particle level set method for improved interface capturing, Journal of Computational Physics, 183 (2002), pp. 83-116.

[7] R. A. Gingold and J. J. Monaghan, Smoothed particle hydrodynamics: theory and applications to non-sperical stars, Monthly Notices of the Royal Astronomical Society, 181 (1977), pp. 375-389.

[8] S. E. Hieber, J. H. Walther, and P. Koumoutsakos, Fluid-Structure Interactions Using rSPH, Conference proceedings, Summer School on Multiscale Modeling and Simulation, Lugano, Switzerland, 2003.

[9] G. A. Holzapfel, Nonlinear solid mechanics:a continuum approach for engineering, WILEY, 2001.

[10] P. Koumoutsakos, Inviscid axisymmetrization of an elliptical vortex, Journal of Computational Physics, 138 (1997), pp. 821-857.

[11] P. Koumoutsakos and A. Leonard, High-Resolution Simulations of the Flow around an Impulsively Started Cylinder Using Vortex Methods, Journal of Fluid Mechanics, 296 (1995), pp. 1-38.

[12] W. E. Lorensen and H. E. Cline, Marching cubes: A high resolution 3D surface construction algorithm, Conference proceedings, 14th annual conference on Computer graphics an interactive techniques, 1987.
[13] L. B. Lucy, Numerical Approach to Testing of Fission Hypothesis, Astronomical Journal, 82 (1977), pp. 1013-1024.
[14] J. J. Monaghan, Smoothed particle hydrodynamics, Annual Review of Astronomy and Astrophysics, 30 (1992), pp. 543-574.
[15] A. Nava, E. Mazza, F. Kleinermann, N. J. Avis, and M. J., Determination of the mechanical properties of soft human tissues through aspiration experiments, Conference proceedings, MICCAI 03, Montreal, Canada, 2003.
[16] P. W. Randles and L. D. Libersky, Smoothed particle hydrodynamics: Some recent improvements and applications, Computer Methods in Applied Mechanics and Engineering, 139 (1996), pp. 375-408.
[17] P. W. Randles and L. D. Libersky, Normalized SPH with stress points, International Journal for Numerical Methods in Engineering, 48 (2000), pp. 1445-1462.
[18] G. Szeleky, C. Brechbler, R. Hutter, A. Rhomberg, and P. Schmidt, Modelling of soft tissue deformation for laparoscopic surgery simulation, medical image computing and computer-assisted intervention, Conference proceedings, MICCAI '98, Cambridge, MA, 1998.
[19] D. Terzopoulous and K. Fleischer, Deformable Models, The Visual Computer, 4 (1988), pp. 306-331.

Fig. 1 Deformation test case without remeshing having an initial particle of 0.05 (top) and 0.01 (bottom).

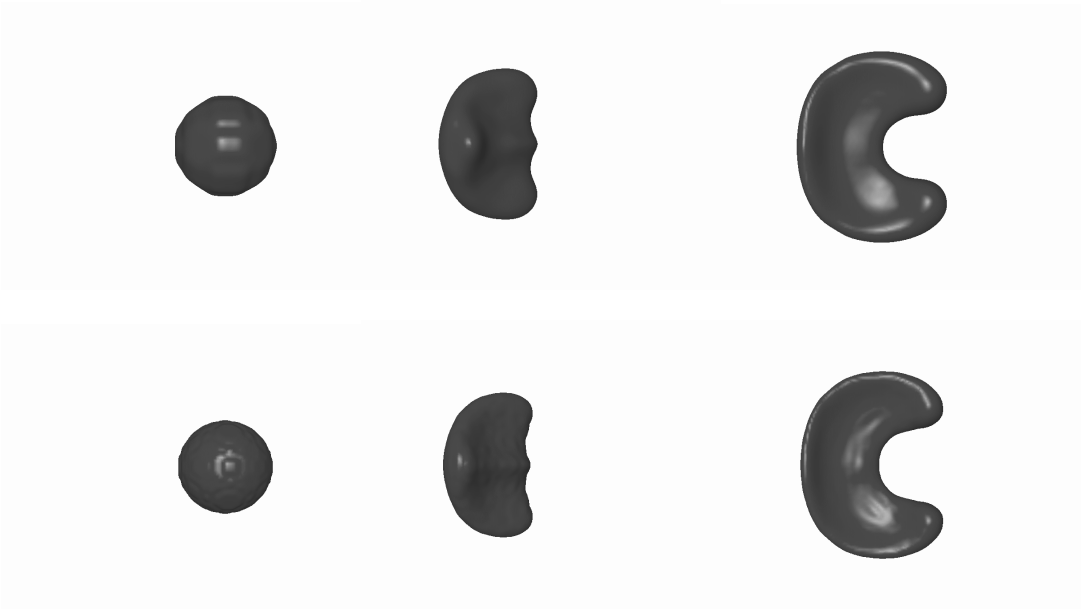

Fig. 2 Deformation test case with remeshing having an initial particle spacing of 0.05 (top) and 0.01 (bottom).

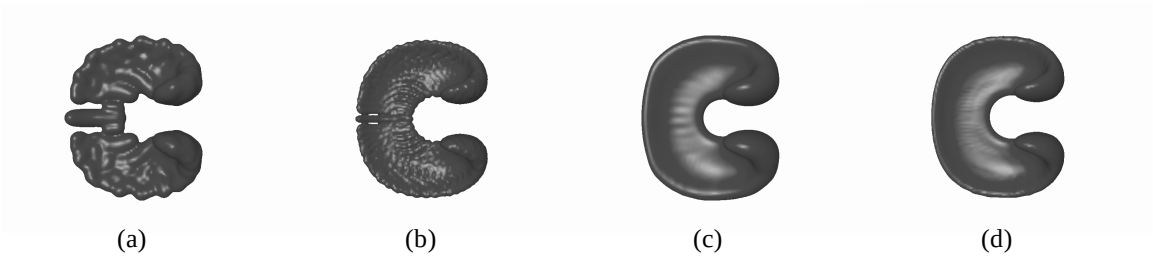

(a) (b) (c) (d)

Fig. 3 Surfaces at T=0.8 with an initial particle spacing of 0.05 (a) and 0.01 (b) without remeshing, and with remeshing (c), (d).

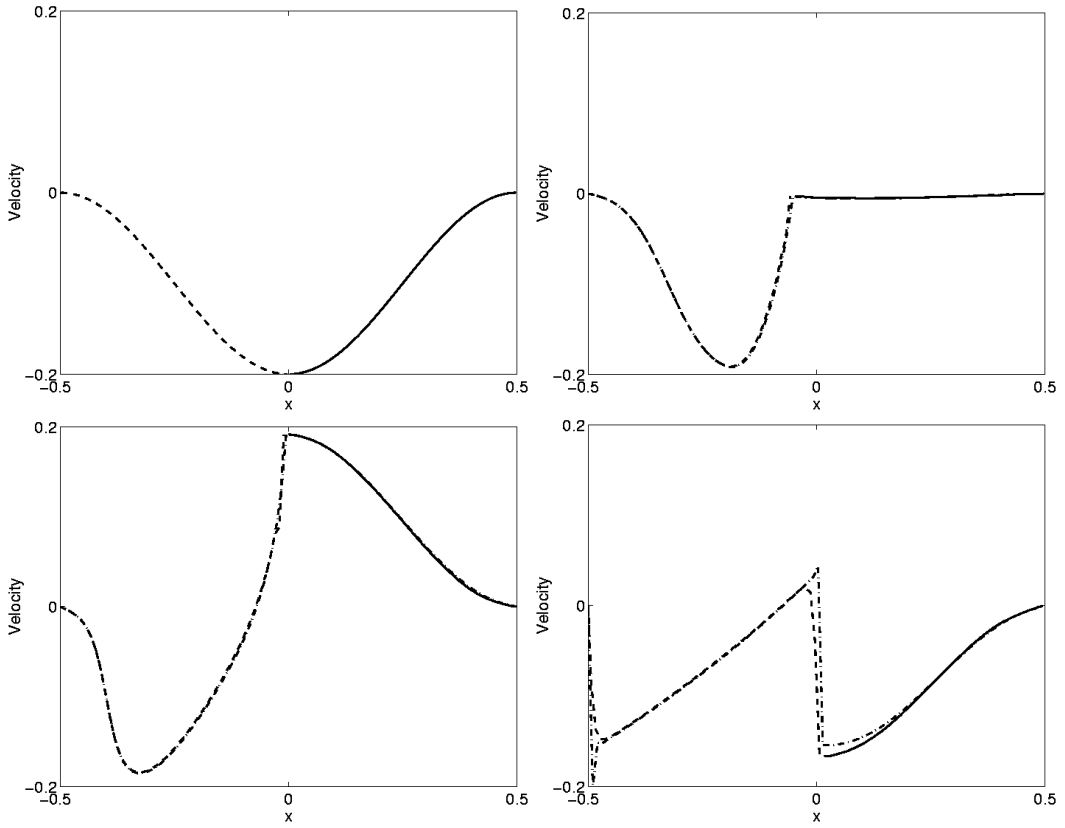

Fig. 4 Fluid-solid interactions. Velocity profiles t=0.0, 0.5, 1.0 and 2.0 of the rSPH solution using 100 particles (fluid --, solid -) and the ALE solution (. -) [8]

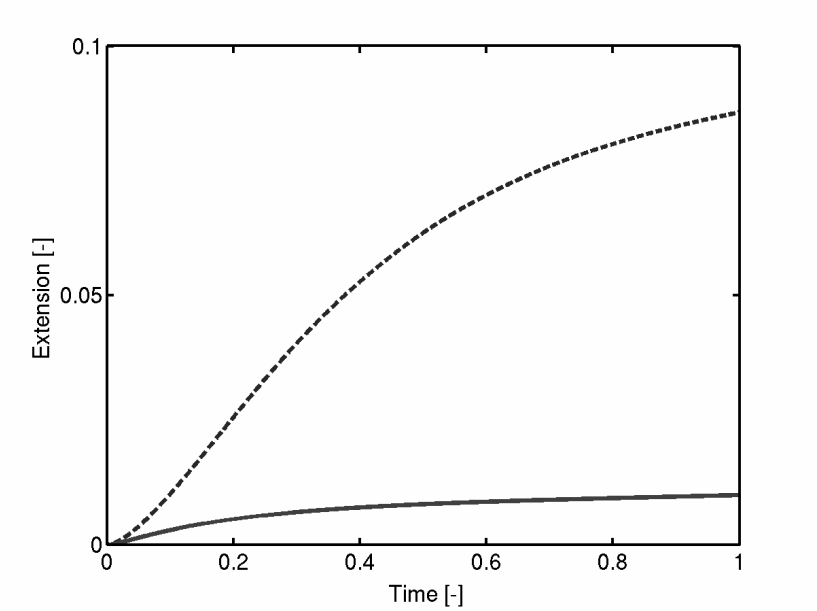

Fig. 5 The computed extecsion (normalized displacement) of the tensile test for the kidney (--) and liver (-) material.

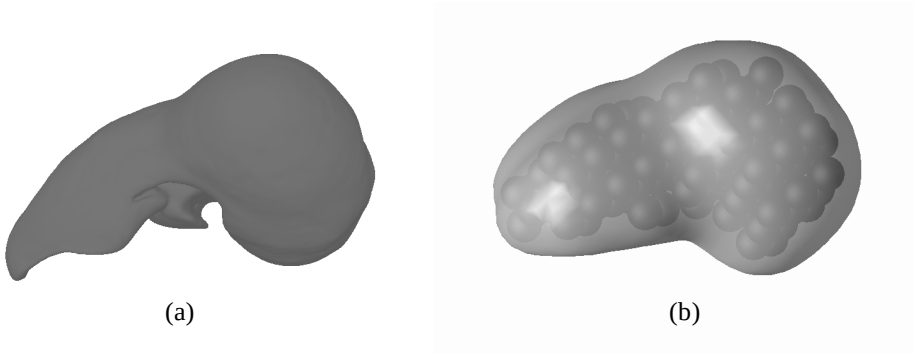

(a) (b)

Fig. 6 The original liver topology (a), the virtual liver with its particle representation (b) using 144 particles.

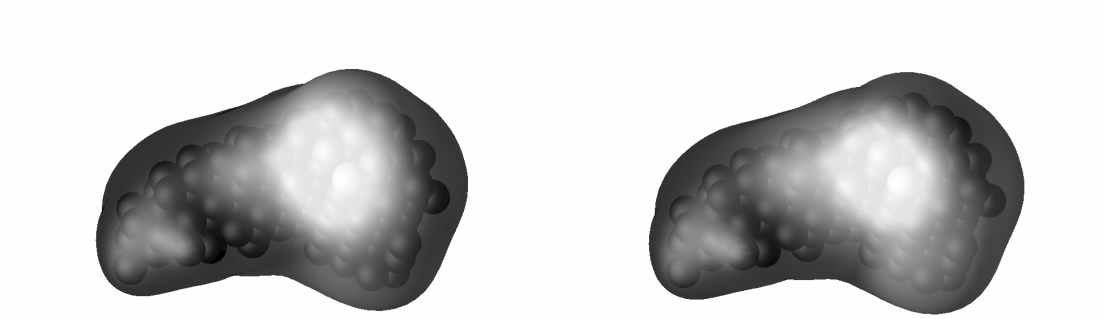

(a) (b)

Fig. 7 The virtual liver with its particle representation (144 particles) under a local mechanical load. The grayscale of the surface corresponds to the local normal strain (a) and shear strain (b)